Eur. Phys. J. B (2012) 85: 301
DOI: 10.1140/epjb/e2012-30236-6

THE EUROPEAN PHYSICAL JOURNAL B

Regular Article

Electronic and transport properties of a biased multilayer hexagonal boron nitride

K. Tang[1,a], Z.Y. Ni[1], Q.H. Liu[1], R.G. Quhe[1], Q.Y. Zheng[1], J.X. Zheng[1,2], R.X. Fei[1], Z.X. Gao[1], and J. Lu[1,b]

[1] State Key Laboratory of Mesoscopic Physics and Department of Physics, Peking University, No. 5 Yiheyuan Road Haidian District, Beijing 100871, P.R. China
[2] Academy for Advanced Interdisciplinary Studies, Peking University, No. 5 Yiheyuan Road Haidian District, Beijing 100871, P.R. China

Received 16 March 2012 / Received in final form 5 June 2012
Published online 5 September 2012 –

Abstract. We explore the electronic and transport properties out of a biased multilayer hexagonal boron nitride (h-BN) by first-principles calculations. The band gaps of multilayer h-BN decrease almost linearly with increasing perpendicular electric field, irrespective of the layer number N and stacking manner. The critical electric filed (E_0) required to close the band gap decreases with the increasing N and can be approximated by $E_0 = 3.2/(N-1)$ (eV). We provide a quantum transport simulation of a dual-gated 4-layer h-BN with graphene electrodes. The transmission gap in this device can be effectively reduced by double gates, and a high on-off ratio of 3000 is obtained with relatively low voltage. This renders biased MLh-BN a promising channel in field effect transistor fabrication.

1 Introduction

Stimulated by the isolation of graphene from graphite by micromechanical cleavage, other single layer materials such as single layer hexagonal boron nitride (h-BN) are also isolated this way [1]. Later, the successful fabrication of large-area (several cm^2) h-BN layers [2] by chemical vapor deposition opened up the possibility of mass production of this new material. Single layer h-BN is a graphene-like structure with a small lattice mismatch [3–6]. Both theoretical [5,7] and experimental [8–10] studies show that single layer h-BN and its multilayer structures are electrically insulating, with large band gaps of 4−8 eV. h-BN layers have high purity, as well as thermal and chemical stabilities. Due to these characteristics, h-BN layers have found wide applications in electronic devices. For example, they are ideal materials to isolate graphene from surface-imperfect common SiO_2 dielectrics, and the carrier mobility of h-BN supported graphene is an order of magnitude higher than the SiO_2-supported one [11]. In addition, a band gap can be created in semi-metallic graphene [12,13], when graphene is placed on or sandwiched between h-BN sheets. Nevertheless, h-BN sheets themselves have not yet been considered as a channel of FET fabrication because the large band gap makes it difficult to tune the source-drain current using the gate voltage.

A vertical electric field cannot modify the band gap of monolayer graphene or single layer h-BN. However, theoretical [14,15] and experimental [16,17] research has found that the band gap of multilayer graphene (MLG) can be tuned by perpendicular electric field. This naturally leads us to consider whether similar tactics will work on MLG's BN counterpart: multilayer hexagonal boron nitride (MLh-BN). If the band gap can be reduced to 1−2 eV, MLh-BN would serve as a semiconductor with a band gap appropriate for FET fabrication. Theoretical calculations have predicted that the band gap of bilayer h-BN can be reduced and ultimately closed under a perpendicular electric field [5]. Unfortunately, the required field strength to reduce the band gap to 1−2 eV is too large (about 1 V/Å) and thus prevents its application in real FETs. In this context, we consider whether MLh-BN with additional layers can solve this problem. To the best of our knowledge, the transport properties of MLh-BN remain open, and it is desirable to explore the transport properties of MLh-BN.

In our work, we use density functional theory (DFT) to study how a perpendicular electric field alters the band gap of MLh-BN sheets of three of the most stable stacking patterns [5]. The dependence of the electric field required to close the band gap on the number of layers and stacking pattern is also investigated. Moreover, we provide an ab initio quantum transport simulation of dual-gated MLh-BN with graphene electrodes. We verify that the transmission gap can be effectively reduced by an electric field and that a large on-off ratio is available by applying a small gate voltage.

[a] e-mail: tangkechao1010@hotmail.com
[b] e-mail: jinglu@pku.edu.cn

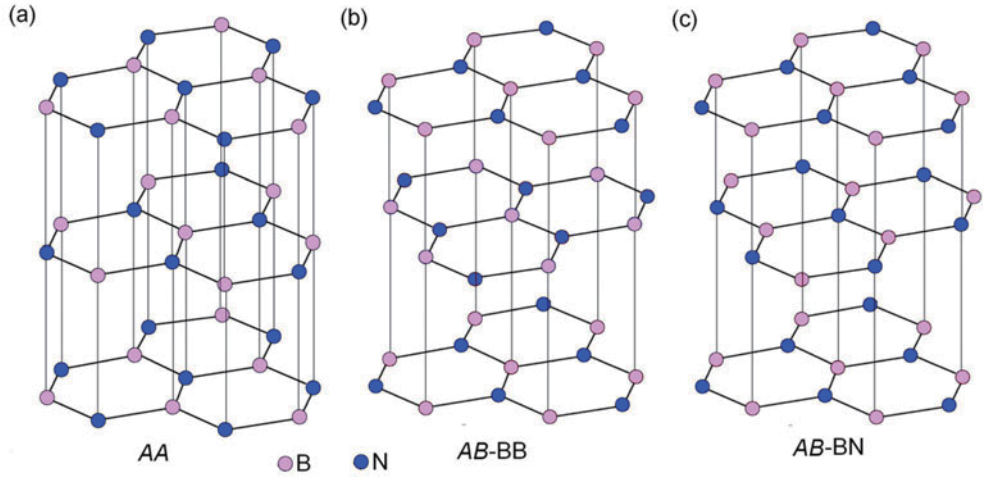

Fig. 1. (Color online) Lattice structures of the stable stacking systems of multilayer BN sheets.

2 Model and method

Two dimensional structures of multilayer hexagonal boron nitride (MLh-BN) are simulated within a hexagonal supercell. In our work, we focus on MLh-BN with three types of stacking patterns, labeled as *AA*, *AB-BB* and *AB-BN*, respectively (Fig. 1), since their corresponding bilayers are predicted to be the most stable amongst all bilayer systems. We take lattice parameter $a = b = 2.48$ Å and the distance between consecutive layers $d = 3.22$ Å [5], providing that these parameters in MLh-BN are the same as those in their bilayer h-BN. The electronic structure of MLh-BN is calculated using the triple numerical basis set plus polarisation (TNP) implemented in the Dmol [3] package [18]. The energy dispersion in wave vector space is obtained by applying the self-consistent field method (SCF) in the first Brillouin zone sampled on a $15 \times 15 \times 1$ Monkhorst-Pack k-points grid [19].

The electric field can be included as an additional sawtooth potential along the z-direction with a discontinuity at the mid plane of the vacuum region of the supercell. To avoid the discontinuity of the sawtooth potential, as well as the interaction with spurious replicas along the z-direction, we set $c = N \times 5 + 10$ for MLh-BN with N layers and place the subject structures in the bottom part of the supercell.

A dual-gate two-probe model is built to simulate the transport of a 4-layer h-BN. For simplicity, 4-layer graphene is used for the electrodes, which is connected to the 4-layer BN in the scattering region by covalent bonds. This configuration of the graphene-BN junction has already been theoretically studied [20] and experimentally fabricated [21]. Transportation properties are calculated using DFT coupled with the non-equilibrium Green's function (NEGF) formalism implemented in the ATK 11.2 package [22–24] The single zeta (SZ) basis set is employed. The k-points of the electrodes and central region, generated by the Monkhorst-Pack scheme, are set to $1 \times 50 \times 50$ and $1 \times 50 \times 1$, respectively. We use generalised gradient approximation (GGA) of the Perdew-Burke-Ernzerhof (PBE) form [25] for the exchange-correlation functional throughout the calculation. The temperature is set to 300 K. The current is calculated using the Landauer-Büttiker formula [26]:

$$I(V_g, V_{bias}) = \frac{2e}{h} \int_{-\infty}^{+\infty} \{T_{V_g}(E, V_{bias})[f_L(E - \mu_L) - f_R(E - \mu_R)]\} dE, \quad (1)$$

where $T_{V_g}(E, V_{bias})$ is the transmission probability at a given gate voltage V_g and bias voltage V_{bias}, $f_{L/R}$ is the Fermi-Dirac distribution function for the left (L)/right (R) electrode, and μ_L/μ_R is the electrochemical potential of the L/R electrode.

3 Results and discussion

Figure 2 shows the band gaps of 4-layer h-BN with the *AA* stacking mode subject to perpendicular electric fields of $E_\perp = 0, 0.51$, and 0.98 V/Å. A reduction in the band gap with the increasing $E_\perp$ is apparent. The corresponding band gaps are $\Delta = 4.83$, 2.46 and 0 eV, respectively. Figure 3 shows the band gap (Δ) of 4-layer h-BN with three stacking modes as a function of $E_\perp$. From this figure, it can be seen that the band gap decreases almost linearly with increasing $E_\perp$ before finally closing. The effects of the stacking mode are not very significant and the critical electric field E_0 ranges from 0.9 to 1.2 V/Å. An approximately linear decrease in Δ with $E_\perp$ and a weak dependence on the stacking mode are also found in the other six MLh-BNs. Table 1 gives the electric field required to reduce the band gap to half ($E_{1/2}$) and E_0 for MLh-BN with $N = 2-8$ under the three stacking modes. It is apparent that the larger the N, the smaller the $E_{1/2}$ and E_0. For example, in *AA* stacked MLh-BN, $E_{1/2}$ and E_0 decrease from 1.8 V/Å to 0.38 V/Å and from 3.6 V/Å to 0.72 V/Å, respectively, when N increases from 2 to 5. In Figure 4 we plot $E_{1/2}$ of the *AA* stacked MLh-BN as a function of N. This relationship can be fitted

Table 1. The electric field required to reduce the band gap of MLh-BN ($N = 2$ to 8) to half of its original value ($E_{1/2}$) and to zero (E_0). Three stable stacking systems where the number of layer ranges from $N = 2$ to 8 are investigated. The E_0 values for MLh-BN with $N = 6$ to 8 in these stacking systems are unavailable due to the failure of SCF convergence in our calculations.

N	AA		AB-BB		AB-BN	
	$E_{1/2}$ (V/Å)	E_0 (V/Å)	$E_{1/2}$ (V/Å)	E_0 (V/Å)	$E_{1/2}$ (V/Å)	E_0 (V/Å)
2	1.80	3.60	1.66	3.29	1.80	3.60
3	0.87	1.70	0.77	1.54	0.77	1.54
4	0.51	0.98	0.49	0.93	0.48	0.93
5	0.38	0.72	0.35	0.66	0.37	0.71
6	0.32	—	0.29	—	0.30	—
7	0.28	—	0.26	—	0.26	—
8	0.23	—	0.21	—	0.21	—

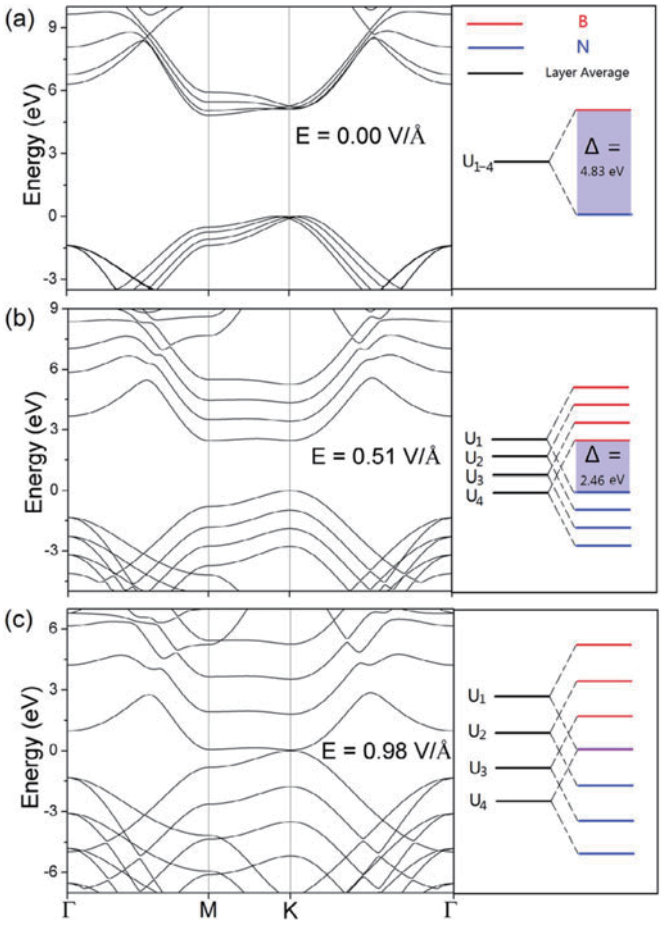

Fig. 2. (Color online) (a-c) Band structures of AA-stacking MLh-BN with 4 layers under perpendicular electric field of 0 V/Å (a), 0.51 V/Å (b) and 0.98 V/Å (c). The right part: illustration of the Stark Effect in 4-layer MLh-BN. U_1, U_2, U_3, and U_4 stand for the average energy levels of each layer.

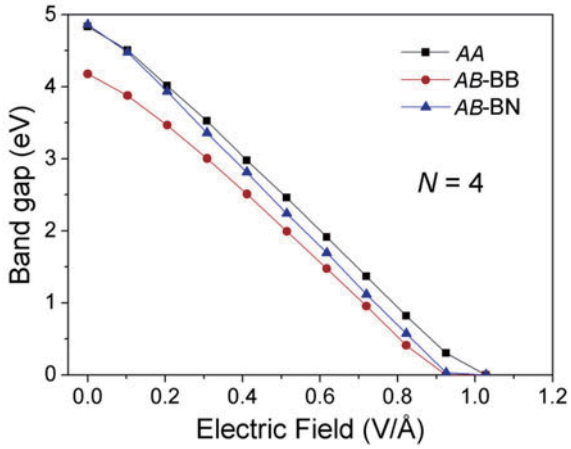

Fig. 3. (Color online) The band gap of 4-layered BN sheets as a function of applied perpendicular electric field.

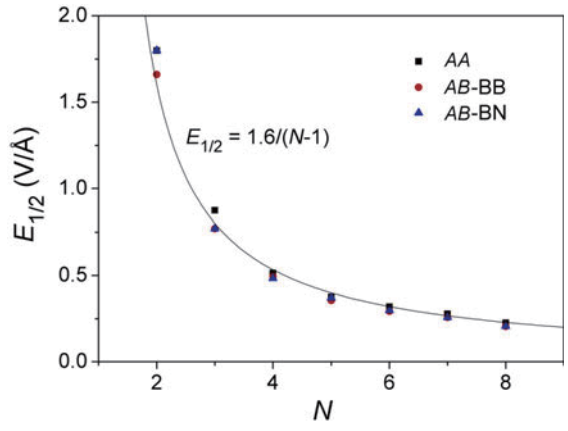

Fig. 4. (Color online) The electric field required to reduce the band gap of multilayer h-BN sheets to half of its original value ($E_{1/2}$) as a function of the number of layers (N). We also provide a fitting function (solid line) to estimate the cases with more layers.

by $E_{1/2} = 1.6/(N-1)$ in units of V/Å. Our results agree well with a very recent work on MLh-BN, which also found that E_0 decreases as N increases [27]. For example, the estimated E_0 of 8-layer AA-stacked h-BN is approximately 0.46 V/Å from a linear extrapolation, while the calculated E_0 is 0.41 V/Å in the referenced work.

The closing of the band gap in MLh-BN under a perpendicular electric field can be explained within a simple tight binding (TB) model. For MLh-BN with N layers, $2N$ Bloch wave functions, constructed from $2p_z$ orbitals

of boron and nitride atoms in each layer, are taken as the basis functions,

$$\psi_{\vec{k}}^{B_j} = \sum_{\vec{R}_{B_j}} e^{i\vec{k}\cdot\vec{R}_{B_j}} \Phi_{B_j}(\vec{r} - \vec{R}_{B_j}), \quad (2)$$

$$\psi_{\vec{k}}^{N_j} = \sum_{\vec{R}_{N_j}} e^{i\vec{k}\cdot\vec{R}_{N_j}} \Phi_{N_j}(\vec{r} - \vec{R}_{N_j}) \quad j = 1, 2, 3 \ldots N, \quad (3)$$

where $\vec{R}_{B_j}$ and $\vec{R}_{N_j}$ are the positions of boron and nitride atoms in the jth layer, while Φ_{B_j} and Φ_{N_j} are the $2p_z$ orbitals in respective atoms. In our simple TB description, we only consider interactions amongst nearest atoms. Under this basis, the Hamiltonian for MLh-BN with N layers is given by:

$$H_N = \begin{bmatrix} D_1 & V_1 & & & \\ V_1^+ & D_2 & V_2 & & \\ & V_2^+ & D_3 & \ddots & \\ & & \ddots & \ddots & V_{N-1} \\ & & & V_{N-1}^+ & D_N \end{bmatrix} \quad D_j = \begin{bmatrix} U_{b_j} & \gamma_0 f \\ \gamma_0 f & U_{n_j} \end{bmatrix}$$

$$(j = 1, 2, 3 \ldots N). \quad (4)$$

For AA systems: $V_j = \begin{bmatrix} 0 & \gamma_{bn} \\ \gamma_{bn} & 0 \end{bmatrix}$

$$(j = 1, 2, 3 \ldots N). \quad (5)$$

For AB-BB systems: $V_j = \begin{bmatrix} \gamma_{bb} & 0 \\ 0 & 0 \end{bmatrix}$

$$(j = 1, 2, 3 \ldots N). \quad (6)$$

For AB-BN systems: $V_j = \begin{bmatrix} 0 & \gamma_{bn} \\ 0 & 0 \end{bmatrix}$ when j is odd

and $V_j = \begin{bmatrix} 0 & 0 \\ \gamma_{bn} & 0 \end{bmatrix}$ when j is even $(j = 1, 2, 3 \ldots N)$ (7)

$$f(k_x, k_y) = e^{ik_x a/\sqrt{3}} + 2e^{-ik_x a/2\sqrt{3}} \cos k_y a/2, \quad (8)$$

where γ_0, γ_{bn} and γ_{bb} describe the nearest B-N coupling within each layer, the nearest B-N coupling in different layers, and the nearest B-B coupling in different layers, respectively, while U_{bj} and U_{nj} represent the on-site energy of B and N in the jth layers. Under electric field, U_{bj} and U_{nj} can be denoted as

$$U_{bj} = U_b + \frac{E}{\varepsilon} d(j-1),$$
$$U_{nj} = U_n + \frac{E}{\varepsilon} d(j-1) (j = 1, 2, 3 \ldots M), \quad (9)$$

in which E is the applied electric field, d is the distance between neighboring layers, U_b the on-site energy of B, U_n the on-site energy of N, and ε the effective dielectric coefficient of MLh-BN. We introduce ε because external electric field would be partly screened in MLh-BN due to charge redistribution. The band structure of MLh-BN can be obtained by diagonalising this $2N \times 2N$ Hamiltonian matrix as a function of k.

Since MLh-BN has similar structure and bonding pattern to multilayer graphene (MLG), γ_{bn} and γ_{bb} can be estimated as being comparable with the interlayer coupling parameter (γ_{cc}) in MLG, which is about 0.4 eV. However, unlike MLG, there is a large potential difference ($U_{bn} =\mid U_b - U_n \mid$) between the boron atoms and nitride atoms in MLh-BN, estimated to be around 5 eV [28]. In contrast with MLG, where γ_{cc} is important in determining the band structures around the Fermi level [15], the zero-field band gap in MLh-BN is actually caused by U_{bn}, while γ_{bn} and γ_{bb}, which are much smaller than U_{bn}, only modify the band structures slightly. This explains why the three systems of MLh-BN have similar band gap behaviours, while the band structures in MLG are largely dependent on the stacking patterns. By omitting γ_{bn} and γ_{bb}, the Hamiltonians of MLh-BN for all stacking orders can be simplified as:

$$H_N = \begin{bmatrix} D_1 & & & & \\ & D_2 & & & \\ & & D_3 & & \\ & & & \ddots & \\ & & & & D_N \end{bmatrix} \quad D_j = \begin{bmatrix} U_{bj} & \gamma_0 f \\ \gamma_0 f & U_{nj} \end{bmatrix}$$

$$(j = 1, 2, 3 \ldots N), \quad (10)$$

$$U_{bj} = U_b + \frac{E}{\varepsilon} d(j-1) \quad U_{nj} = U_n + \frac{E}{\varepsilon} d(j-1)$$
$$(j = 1, 2, 3 \ldots N). \quad (11)$$

In the absence of a perpendicular electric field, the conduction bands and valence bands of MLh-BN, formed by B orbitals and N orbitals in different layers, respectively, are almost degenerate, leaving a band gap of approximately 5 eV, almost equal to U_{bn} (see Fig. 2a). With the application of an electric field, an energy difference between the layers is introduced, leading to the breaking of degeneracy in valence bands and conduction bands. As the electric field becomes stronger, the valence and conduction bands of atoms on different layers also expand (Fig. 2b), and finally close the band gap between the valence band and the conduction bands (Fig. 2c). This process is actually a showcase of the Stark effect, which is illustrated in the right part of Figure 2. In Figure 2, U_1, U_2, U_3 and U_4 stand for the average energy levels of each layer. ($U_j = (U_{bj} + U_{nj})/2$, $j = 1, 2, 3, 4$). The applied external electric field introduces a potential difference between layers, which breaks the degeneracy of U_1 to U_4 and splits these energy levels. In this way, the energy levels of the B orbitals (red lines) and the N orbitals (blue lines) expand, and thus narrow the energy gap between the B and N orbitals. In light of this model, the closing of the band gap takes place when the energy difference between the top and bottom layer ($\mid U_1 - U_N \mid$) is large enough to negate

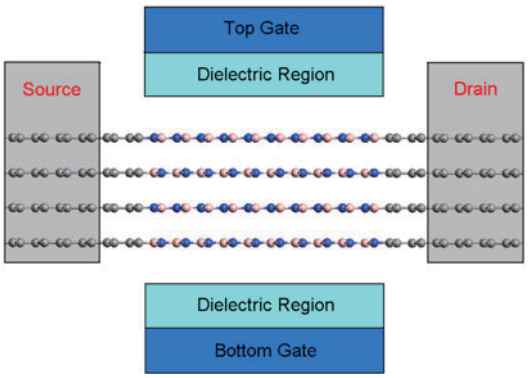

Fig. 5. (Color online) Configuration of our simulated 4-layer BN sheet field effect transistor (AA-stacking).

the potential difference of the B and N atoms. Here we have:

$$\frac{E_0}{\varepsilon} d(N-1) = U_{bn} \tag{12}$$

in which E_0 is the critical electric field, and N is the number of layers. According to this equation, the electric field required to close the band gap in MLh-BN is inversely proportional to $N-1$, the validity of which is supported by the good agreement between the outcome of DFT calculations and the fitting function $E_{1/2} = 1.6/(N-1)$ (that is, $E_0 = 3.2/(N-1)$, due to the linear decrease of Δ with $E_\perp$) (Fig. 4). Furthermore, by setting U_{BN} to 4.8 eV, i.e. equal to the energy gap of unbiased AA-stacking MLh-BN, we extract a constant value of ε of approximately 2.1 in MLh-BN, which is comparable to the dielectric coefficient of bulk h-BN (3–4) [11]. This fitting function can then be used to predict the critical electric field in MLh-BN with more layers. In light of this function, MLh-BN should be more than 32 layers for the critical electric field to fall below 0.1 V/A, the tolerance of SiO_2 dielectrics [29]. In addition, when MLh-BN of a given number of layers is used as a buffer layer between graphene and dielectrics, (a common application in experiments) [11,30], the function is also useful for estimating the upper limit of the electric field that the buffer region can endure.

The model of a double-gated AA-stacking 4-layer boron nitride FET with graphene electrodes is shown in Figure 5. The distance between the two gates is $d_0 = 35.66$ Å in our model, and the thickness of both the top and the bottom dielectric is $d_i = 8$ Å. We set the dielectric constant of the dielectric regions to $\varepsilon = 3.9$, which models SiO_2, and lattice parameters as well as layer distance of the 4-layer boron nitride are taken to be the same asour DFT calculations. In contrast with a single-gated FET, a double-gated device can control the vertical electric field applied on the scattering region and the doping level independently. With the top and bottom gate voltages labeled as V_t and V_b respectively, the vertical electric field applied to the 4-layer boron nitride can be denoted as $E_{gate} = \frac{V_t - V_b}{(d_0 - 2d_i) + 2d_i/\varepsilon}$, while the corresponding total gate voltage is $V_g = V_t + V_b$, reflecting the total doping level. In our work, we first try to reduce the energy gap of 4-layer boron nitride to approximately 1 eV, a size suitable for

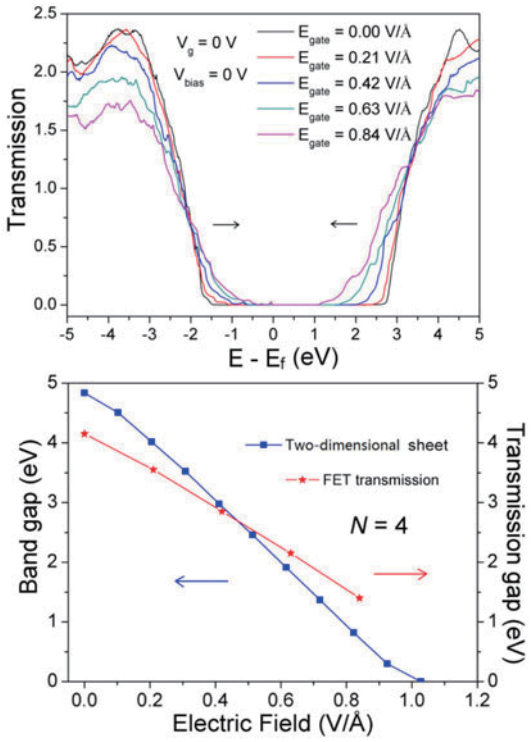

Fig. 6. (Color online) (a) Changes in the transmission spectra of the 4-layer AA-stacking h-BN FET with the increasing electric field. (b) Transmission gap of the 4-layer h-BN FET and the band gap of the 2D 4-layer h-BN sheet as a function of electric field.

FET fabrication, by applying a vertical electric field. On this basis, we then calculate the source-drain current of the FET under different V_g and the on-off ratio with fixed bias voltage (V_{bias}), in order to verify the effectiveness of our FET.

The transmission spectra of the FET under different electric fields are compared in Figure 6a. In the absence of an applied electric field, the transmission spectrum displays a large transmission gap of 4.2 eV, due to the insulating property of the boron nitride in the scattering region. In accordance with the predicted changes in the energy bands, the vertical electric field applied by the double gates reduces the transmission gap of the FET. In Figure 6b we plot the transmission gap of the FET, together with the energy gap of a two-dimensional (2D) boron nitride sheet, as a function of the electric field. The former in general corresponds well with the latter. It is worth noting that in the absence of a perpendicular electric field, the transmission gap is obviously smaller than in the 2D boron nitride sheet, by roughly 0.6 eV. This is probably due to the limited size effect in the source-drain direction, which allows for leaking between the source and drain and thus diminishes the transmission gap. Until now, we have successfully reduced the transmission gap from over 4 eV to approximately 1.4 eV, an appropriate size for a FET device, by applying an electric field of 0.84 V/Å

In Figure 7a we plot the transmission spectra of our gap-reduced FET under different V_g with

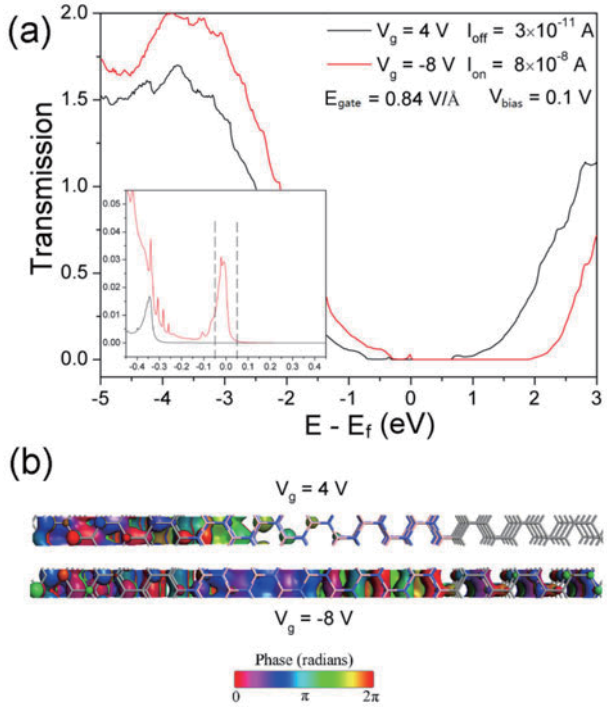

Fig. 7. (Color online) (a) Transmission spectra of the 4-layer AA-stacking BN FET under different gate voltages with fixed electric field and source-drain bias voltage. Inset: a magnified picture of the transmission spectra around the Fermi level. (b) Transmission eigenstates for the off- ($V_g = 4$ V) and on-state ($V_g = -8$ V) at E_f and at the (1, 1/3) point of k-space. The isovalues are 0.4 a.u.

$E_{gate} = 0.84$ V/Å and $V_{bias} = 0.1$ V. In this case, the Dirac points of the source and drain in the FET move to ± 0.05 eV, respectively, forming a bias window (dashed line in Fig. 7a) between them. According to formula (1), the source-drain current can be approximated as the integral of the transmission probability within the bias window, as long as the temperature is not very high. In this way, we can see that an off-state is generated when $V_g = 4$ V, which shifts the transmission spectrum in the negative direction and covers the entire bias window with a transmission gap. On the other hand, a gate voltage of -8 V moves the transmission gap out of the bias window and thus switches the device to the on-state. The difference between the off-state and the on-state is also reflected in the transmission eigenchannel at E_f and at the (0, 1/3) point of k-space, as displayed in Figure 7b. The largest transmission eigenvalue of the off-state is 5.1×10^{-5}, and the corresponding incoming wave function is apparently scattered, so that it is unable to reach the other lead. On the other hand, the largest transmission eigenvalue of the on-state is 0.41, in which case the scattering is weak and much of the incoming wave is able to reach the other lead. Here we obtain a high on/off current ratio of approximately 3000 under $E_{gate} = 0.84$ V/Å at 300 K.

However, some remaining issues concerning 4-layer h-BN-based FET need to be noted. It is obvious that the required electric field to tune the transmission band gap remains too high (0.84 V/Å), far beyond the electric breakdown limit of SiO_2 (0.1 V/Å). However, according to the fitting function obtained, the required electric field would diminish as the number of layers increases, and it is estimated that the electric field to tune the transmission gap to approximately 1 eV would fall below 0.1 V/Å in MLh-BN with 30 layers. Experimental fabrication of a 30-layer MLh-BN is not a difficult task, while theoretical modeling of this system has gone far beyond our computational capacity. In addition, we found that the effective masses of carriers (m) in MLh-BN remain at around $1m_e$ (the mass of a free electron), regardless of stacking manners, number of layers, and the applied electric field. According to the equation $\mu = e\tau/m$, given a fixed time interval between consecutive scatterings (τ), the carrier mobility in materials (μ) is inversely proportional to the effective masses of carriers (m). Therefore, the invariance of m suggests that MLh-BN of all configurations have the same μ, and μ is not compromised by tuning the band gap with the electric field. Finally, we predict the carrier mobility of MLh-BN from available resources. In a recent study, a carrier mobility of 58.8 $cm^2/V\,s$ was measured in zigzag hexagonal boron nitride nanoribbons (h-BNNR) [31]. It is worth noting that μ of a two-dimensional sheet usually diminishes when the sheet is cut into a nanoribbon, since the edge effect in nanoribbons allows for more scatterings and reduces τ. For instance, μ of SiO_2-substrate-supported graphene is as high as 15000 $cm^2/V\,s$ [14], while that of SiO_2-substrate-supported graphene nanoribbons is only 100−200 $cm^2/V\,s$ [32] Extrapolated from the case of graphene, which is similar to h-BN in structure, we estimate that μ of MLh-BN is also about 2 orders of magnitude higher than that of h-BNNR and is approximated to be of the order of 1000 $cm^2/V\,s$. This high carrier mobility makes MLh-BN suitable for the fabrication of high-switching-speed transistors.

4 Conclusion

In summary, using first principles calculations, we have shown that the band gap of MLh-BN decreases with increasing perpendicular electric field and eventually closes at a critical field, which is inversely dependent on the number of layers. With the aid of a simple TB model, these phenomena are successfully explained, and a fitting function is provided to predict the critical field in MLh-BN with an arbitrary number of layers. We also simulate a FET based on MLh-BN, which features a transmission gap tunable by double voltage gates and high on-off ratio, and therefore we propose MLh-BN as a promising channel candidate for FET fabrication. Our work is expected to stimulate the experimental fabrication of FET out of MLh-BN.

This work was supported by the NSFC (Grant No. 10774003), National 973 Projects (No. 2007CB936200, MOST of China), Fundamental Research Funds for the Central Universities, National Foundation for Fostering Talents of Basic Science (No. J0630311), and Program for New Century Excellent Talents in University of MOE of China.

Appendix: Table of content (TOC)

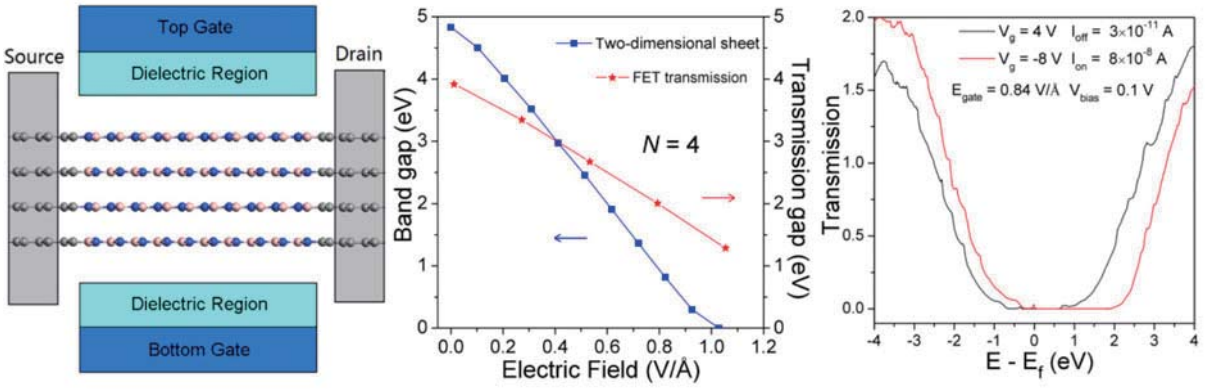

References

1. K.S. Novoselov, A.K. Geim, S.V. Morozov, D. Jiang, M.I. Katsnelson, I.V. Grigorieva, S.V. Dubonos, A.A. Firsov, Nature **438**, 197 (2005)
2. L. Song, L. Ci, H. Lu, P.B. Sorokin, C. Jin, J. Ni, A.G. Kvashnin, D.G. Kvashnin, J. Lou, B.I. Yakobson, P.M. Ajayan, Nano Lett. **10**, 3209 (2010)
3. D. Golberg, Y. Bando, Y. Huang, T. Terao, M. Mitome, C. Tang, C. Zhi, ACS Nano **4**, 2979 (2010)
4. A. Abdellaoui, A. Bath, B. Bouchikhi, O. Baehr, Mater. Sci. Eng. B **47**, 257 (1997)
5. Z.L. Yang, J. Ni, J. Appl. Phys. **107**, 104301 (2010)
6. D. Pacile, J.C. Meyer, C.O. Girit, A. Zettl, Appl. Phys. Lett. **92**, 133107 (2008)
7. R.M. Ribeiro, N.M.R. Peres, Phys. Rev. B **83**, 235312 (2011)
8. V.L. Solozhenko, A.G. Lazarenko, J.P. Petitet, A.V. Kanaev, J. Phys. Chem. Solids **62**, 1331 (2001)
9. K. Watanabe, T. Taniguchi, H. Kanda, Nat. Mater. **3**, 404 (2004)
10. L. Wirtz, A. Marini, A. Rubio, Phys. Rev. Lett. **96**, 126104 (2006)
11. C.R. Dean, A.F. Young, I. Meric, C. Lee, L. Wang, S. Sorgenfrei, K. Watanabe, T. Taniguchi, P. Kim, K.L. Shepard, J. Hone, Nat. Nanotechnol. **5**, 722 (2010)
12. A. Ramasubramaniam, D. Naveh, E. Towe, Nano Lett. **11**, 1070 (2011)
13. R.G. Quhe, J.X. Zheng, G.F. Luo, Q. Liu, R. Qin, J. Zhou, D.P. Yu, S. Nagase, W.N. Mei, Z.X. Gao, J. Lu, NPG Asia Materials **4**, e6 (2012), DOI: 10.1038/am.2012.10
14. K. Tang, R. Qin, J. Zhou, H. Qu, J. Zheng, R. Fei, H. Li, Q. Zheng, Z. Gao, J. Lu, J. Phys. Chem. C **115**, 9458 (2011)
15. A.A. Avetisyan, B. Partoens, F.M. Peeters, Phys. Rev. B **81**, 115432 (2010)
16. J.B. Oostinga, H.B. Heersche, X.L. Liu, A.F. Morpurgo, L.M.K. Vandersypen, Nat. Mater. **7**, 151 (2008)
17. Y.B. Zhang, T.T. Tang, C. Girit, Z. Hao, M.C. Martin, A. Zettl, M.F. Crommie, Y.R. Shen, F. Wang, Nature **459**, 820 (2009)
18. B. Delley, J. Chem. Phys. **92**, 508 (1990)
19. H.J. Monkhorst, J.D. Pack, Phys. Rev. B **13**, 5188 (1976)
20. S. Jungthawan S. Limpijumnong, J.-L. Kuo, Phys. Rev. B **84**, 235424 (2011)
21. M.O. Watanabe, S. Itoh, T. Sasaki, K. Mizushima, Phys. Rev. Lett. **77**, 2846 (1996)
22. ATOMISTIX Toolkit, version 11.2. Quantum Wise A/S: Copenhagen, Denmark
23. J. Taylor, H. Guo, J. Wang, Phys. Rev. B **63**, 121104 (2001)
24. M. Brandbyge, J.L. Mozos, P. Ordejon, J. Taylor, K. Stokbro, Phys. Rev. B **65**, 165401 (2002)
25. J.P. Perdew, K. Burke, M. Ernzerhof, Phys. Rev. Lett. **77**, 3865 (1996)
26. S. Dattan *Electronic Transport in Mesoscopic Systems* (Cambridge University Press, Cambridge, England, 1995)
27. M. Otani, S. Okada, Phys. Rev. B **83**, 073405 (2011)
28. J. Slawinska, I. Zasada, Z. Klusek, Phys. Rev. B **81**, 155433 (2010)
29. E.K. Yu, D.A. Stewart, S. Tiwari, Phys. Rev. B **77**, 195406 (2008)
30. J. Xue, J. Sanchez-Yamagishi, D. Bulmash, P. Jacqu, K. Watanabe, T. Taniguchi, P. Jarillo-Herrero, B.J. LeRoy, Nat. Mater. **10**, 282 (2011)
31. H. Zeng, C. Zhi, Z. Zhang, X. Wei, X. Wang, W. Guo, Y. Bando, D. Golberg, Nano Lett. **10**, 5049 (2010)
32. X. Li, X. Wang, L. Zhang, S. Lee, H. Dai, Science **319**, 1229 (2008)